

## Self-compensation induced high-resistivity in MgZnO

This content has been downloaded from IOPscience. Please scroll down to see the full text.

2017 J. Phys. D: Appl. Phys. 50 065102

(<http://iopscience.iop.org/0022-3727/50/6/065102>)

View [the table of contents for this issue](#), or go to the [journal homepage](#) for more

Download details:

IP Address: 137.189.41.6

This content was downloaded on 13/01/2017 at 02:13

Please note that [terms and conditions apply](#).

# Self-compensation induced high-resistivity in MgZnO

Lishu Liu<sup>1</sup>, Zengxia Mei<sup>1</sup>, Aihua Tang<sup>1</sup>, Huili Liang<sup>1</sup> and Xiaolong Du<sup>1,2</sup>

<sup>1</sup> Key Laboratory for Renewable Energy, Beijing National Laboratory for Condensed Matter Physics, Institute of Physics, Chinese Academy of Sciences, Beijing 100190, People's Republic of China

<sup>2</sup> School of Physical Sciences, University of Chinese Academy of Sciences, Beijing 100190, People's Republic of China

E-mail: [zxmei@iphy.ac.cn](mailto:zxmei@iphy.ac.cn) and [xldu@iphy.ac.cn](mailto:xldu@iphy.ac.cn)

Received 17 August 2016, revised 25 October 2016

Accepted for publication 28 October 2016

Published 12 January 2017



## Abstract

The degradation of conductivity with increased Mg content for  $\text{Mg}_x\text{Zn}_{1-x}\text{O}$  wide bandgap materials has always been a fundamental application-motivated research issue. Herein, the study of self-compensating defects in  $\text{Mg}_x\text{Zn}_{1-x}\text{O:F}$  ( $0 \leq x \leq 0.29$ ) thin films was performed to reveal their influence on increased resistivity. Our observations solidly evidence that the degradation of conductivity is mainly owing to the increased concentration of Zn vacancy ( $V_{\text{Zn}}$ )-related compensating defects in  $\text{Mg}_x\text{Zn}_{1-x}\text{O}$  alloys. The formation enthalpy of intrinsic  $V_{\text{Zn}}$  defects decreases as Mg content ( $x$ ) increases. Thus, the compensation ratio increases from 0.23 at  $x = 0$  to 0.47 at  $x = 0.29$ , resulting in deteriorated conductivity in  $\text{Mg}_x\text{Zn}_{1-x}\text{O}$  alloys. Cathodoluminescence (CL) spectra further confirm higher  $V_{\text{Zn}}$  concentrations with increased Mg content. The electron transport is demonstrated to be dominated by an ionized scattering mechanism. Formation of  $F_{\text{O}}^+V_{\text{Zn}}^{2-}$  complexes could reduce the concentration of ionized scattering centers and thus increase mobility. These results clarify the reason of increasingly high resistivity in  $\text{Mg}_x\text{Zn}_{1-x}\text{O}$ , which is a long-sought-after physics problem in this area, and provide crucial information on controlling the conductivity of  $\text{Mg}_x\text{Zn}_{1-x}\text{O}$  alloys.

Keywords: Zn vacancy, formation enthalpy, MgZnO, electron transport

 Online supplementary data available from [stacks.iop.org/JPhysD/50/065102/mmedia](http://stacks.iop.org/JPhysD/50/065102/mmedia)

(Some figures may appear in colour only in the online journal)

## 1. Introduction

Transparent conducting oxides, an important class of materials for various optoelectronic devices, have been studied and applied extensively in the field of liquid crystal displays, organic light emitting diodes, and thin solar cells [1, 2]. Compared to the most widely used indium tin oxides, ZnO is highlighted with a combination of abundant natural reservation, nontoxicity, and high radiation resistance [1, 3, 4]. Moreover, the bandgap of ZnO can be delicately tuned by alloying with MgO, from 3.37 eV to 6.3 eV, which is of great importance in optimizing the performance of ultraviolet photodetectors, transparent conductive electrodes, thin solar cells, etc [5–8]. Similar to ZnO itself, MgZnO can be  $n$ -type doped by substituting the cation lattice atoms with Al, Ga, or

In [9–11], and substituting the anion lattice atoms with F [12]. However, a substantial and undesired decrease in both the carrier concentration ( $n$ ) and the electron mobility ( $\mu$ ) is observed with increased Mg content, resulting in a rapid decrease in conductivity [9–11]. For example, in our previous work on F-doped  $\text{Mg}_x\text{Zn}_{1-x}\text{O}$ ,  $n$  decreased by a factor of three and  $\mu$  decreased by a factor of ten, yielding a 30-fold decrease in conductivity as Mg content increases from  $x = 0$  to 0.3 [12].

Although the degradation of conductivity in  $\text{Mg}_x\text{Zn}_{1-x}\text{O}$  alloys is widely observed [9–11], no consensus has yet been reached on the fundamental issue. For the decrease in  $n$ , researchers have suggested an increasing donor activation energy owing to either a larger effective mass [10, 13] or change of band structure [14]. A lowering of the active donor concentration attributed to composition enrichment has

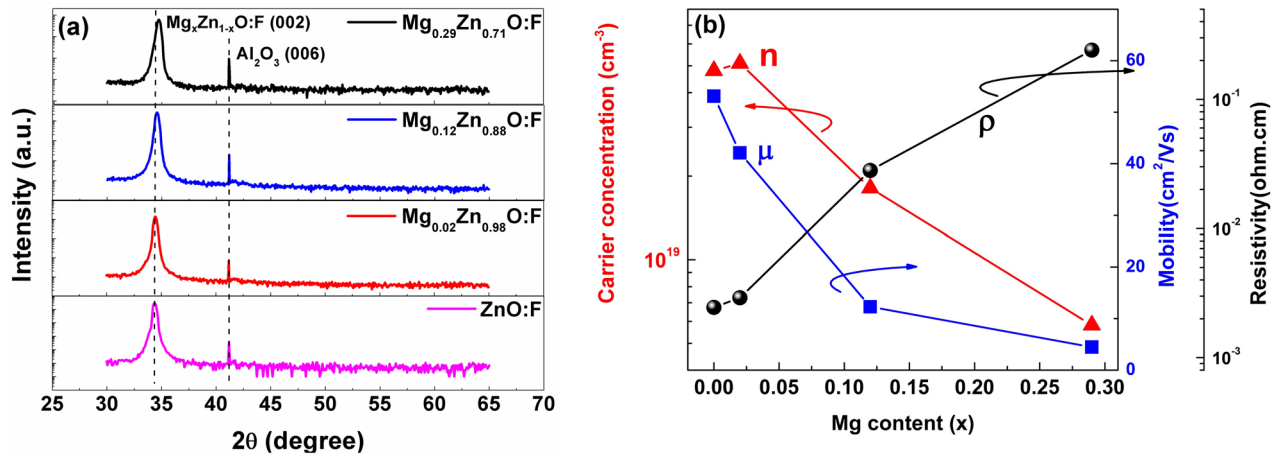


Figure 1. (a) XRD  $\theta$ - $2\theta$  curves and (b) electrical properties of  $\text{Mg}_x\text{Zn}_{1-x}\text{O:F}$  ( $0 \leq x \leq 0.29$ ) at room temperature.

been also reported [13, 15]. As mentioned above,  $\mu$  decreased from  $42 \text{ cm}^2 \text{ V}^{-1} \text{ s}^{-1}$  for F-doped ZnO to  $3.6 \text{ cm}^2 \text{ V}^{-1} \text{ s}^{-1}$  for F-doped  $\text{Mg}_{0.3}\text{Zn}_{0.7}\text{O}$  [12]. Even under the assumption that a fairly large increase of the effective mass from  $0.3m_0$  for ZnO to  $0.6m_0$  for  $\text{Mg}_{0.3}\text{Zn}_{0.7}\text{O:F}$ , an additional decrease of  $\mu$  by a factor of about five must be carefully considered. This has been attributed to alloy scattering [11, 16], impurity scattering [13], and grain boundary scattering [17]. Since the degradation of conductivity with increased Mg content has largely impeded the application of  $\text{Mg}_x\text{Zn}_{1-x}\text{O}$ -based devices, it is highly desirable to understand the origin.

In this letter, the study of native defects in  $\text{Mg}_x\text{Zn}_{1-x}\text{O:F}$  ( $0 \leq x \leq 0.29$ ) thin films was performed. It is demonstrated via theoretical analysis and experimental verification that a self-compensation mechanism is responsible for the deteriorated conductivity in  $\text{Mg}_x\text{Zn}_{1-x}\text{O}$  alloys. The formation enthalpy of Zn vacancy ( $V_{\text{Zn}}$ )-related compensating acceptors decreases with increased Mg content ( $x$ ). Therefore, the compensation ratio increases from 0.23 at  $x = 0$  to 0.47 at  $x = 0.29$ , resulting in the deterioration of conductivity in  $\text{Mg}_x\text{Zn}_{1-x}\text{O}$  alloys. Cathodoluminescence (CL) measurements further confirm higher  $V_{\text{Zn}}$  concentrations with increased Mg content. The electron transport is demonstrated to be mainly limited by ionized impurity scattering. Formation of  $F_{\text{O}}^+ - V_{\text{Zn}}^{2-}$  complexes could reduce the concentration of ionized scattering centers and thus increase  $\mu$  from  $10 \text{ cm}^2 \text{ V}^{-1} \text{ s}^{-1}$  to  $14 \text{ cm}^2 \text{ V}^{-1} \text{ s}^{-1}$  for  $\text{Mg}_{0.12}\text{Zn}_{0.88}\text{O:F}$ . These results clarify the reason of increasingly high resistivity in  $\text{Mg}_x\text{Zn}_{1-x}\text{O}$ , which is a long-sought-after physics problem in this area.

## 2. Experiments

$\text{Mg}_x\text{Zn}_{1-x}\text{O:F}$  samples were synthesized on sapphire (0001) substrates by radio-frequency plasma-assisted molecular beam epitaxy (rf-MBE) with a base pressure of  $\sim 10^{-10}$  mbar. The commercially available  $\text{ZnF}_2$  powder (99.995%, Alfa Aesar) chosen as the doping source was firstly purified and solidified to exclude the possibility of the incorporation of unwanted impurities, and to meet the strict requirements of rf-MBE the growth process. More growth details can be found

elsewhere [12, 18]. Reflection high-energy electron diffraction (RHEED) was utilized *in situ* to monitor the evolution of crystalline structure and surface morphology of all epilayers (see figure S1 and additional graphs in supplemental material<sup>3</sup>) ([stacks.iop.org/JPhysD/50/065102/mmedia](http://stacks.iop.org/JPhysD/50/065102/mmedia)). The bandgaps of  $\text{Mg}_x\text{Zn}_{1-x}\text{O:F}$  samples were determined via room-temperature transmittance spectroscopy (Cary 5000 System) to be 3.31 eV, 3.34 eV, 3.59 eV, and 4.08 eV, respectively (see figure S2 in supplemental material<sup>4</sup>). According to the standard bowling equation [19], i.e.  $E_g(\text{Mg}_x\text{Zn}_{1-x}\text{O}) = (1-x) \times E_g(\text{ZnO}) + x \times E_g(\text{MgO}) - 2.01 \times x(1-x)$ , the Mg content ( $x$ ) is estimated to be 0, 0.02, 0.12, and 0.29, respectively. Here,  $E_g(\text{Mg}_x\text{Zn}_{1-x}\text{O})$ ,  $E_g(\text{ZnO})$ , and  $E_g(\text{MgO})$  denote the bandgaps of  $\text{Mg}_x\text{Zn}_{1-x}\text{O}$ , ZnO, and MgO, respectively. X-ray diffraction (XRD) was performed using Cu  $K\alpha$  radiation (Empyrean System).  $F$  concentration was determined by secondary ion mass spectroscopy (SIMS) using a Hiden MAXIM Analyser. The electrical properties of films were characterized by temperature-dependent Hall (TDH) measurements using a Lakeshore 7604 system and a HL5500PC Hall effect measurement system at low and high temperature, respectively. CL was used to evaluate the energy levels of defects in samples (Quanta 400 FEG system). Electron beams with incident energy  $E_B = 5 \text{ keV}$  excited electron-hole pairs for peak CL excitation depth  $U_0 = \sim 100 \text{ nm}$  for samples at room temperature in an ultra-high vacuum.

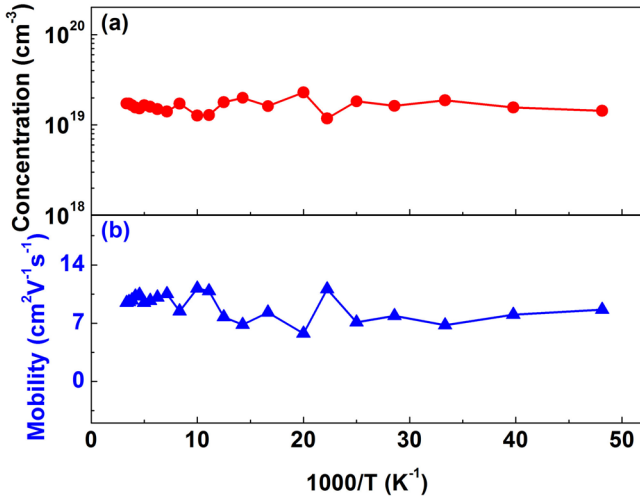
## 3. Results and discussion

Figure 1(a) illustrates the XRD  $\theta$ - $2\theta$  curves of the F-doped samples. The peaks diffracted from wurtzite  $\text{Mg}_x\text{Zn}_{1-x}\text{O:F}$  (002) planes shift toward larger angles, implying a gradual increase in Mg content in these films. Importantly, the appearance of the only (002)-related peaks without any sign of cubic  $\text{MgZnO:F}$  existence confirms the single wurtzite phase, consistent with *in situ* RHEED findings (figure S1 in the supplemental material<sup>5</sup>). Although the above results seem to indicate

<sup>3</sup> See supplemental material for additional graphs.

<sup>4</sup> See footnote 3.

<sup>5</sup> See footnote 3.



**Figure 2.** Temperature-dependent Hall measurements showing (a) carrier concentrations and (b) mobility for  $\text{Mg}_{0.12}\text{Zn}_{0.88}\text{O:F}$ .

that the crystalline structure was little affected by Mg content, the electrical properties of these films, on the other hand, were largely tuned by the incorporation of Mg. As illustrated in figure 1(b),  $n$  and  $\mu$  decreased by a factor of  $\sim 8$  and  $\sim 12$  from  $x = 0$  to  $x = 0.29$ , respectively, resulting in a two orders of magnitude increase in resistivity.

Since the effect of Mg incorporation was mainly reflected in the electrical properties, we will first take  $\text{Mg}_{0.12}\text{Zn}_{0.88}\text{O:F}$  as a typical sample for further electrical analysis. The film was characterized by the TDH using the van der Pauw method in a magnetic field of 5 kG and a temperature range of 20–300 K. The plots of  $n$  and  $\mu$  as a function of temperature are shown in figure 2. It should be noted that  $n$  is essentially temperature independent in the whole range. According to Arrhenius analysis [20, 21], the activation energy ( $E_D$ ) is rather small, indicating that F is indeed a shallow donor in  $\text{Mg}_{0.12}\text{Zn}_{0.88}\text{O}$  and the sample is degenerately doped. Although  $E_D$  of F dopants is small, the measured doping efficiency is low. Specifically,  $n$  is less than 20% of the F concentration. SIMS measurements do not manifest any impurities except F with concentrations larger than  $10^{19} \text{ cm}^{-3}$  in the alloy films. Thus, we reject that unintended extrinsic compensating acceptor dopants account for the observed doping efficiency at this low level. Another possible cause for the low doping efficiency is second phase inclusions, but the structural measurements on the film suggest that this is not the case. As illustrated in XRD (figure 1(a)) and RHEED observations (figure S1), the film is highly epitaxial and has no sign of secondary crystalline or amorphous phases.

Another important mechanism that could lead to the deterioration of doping efficiency with increased Mg content is the formation of self-compensating acceptors. Growing evidence suggests that  $V_{\text{Zn}}$  is the dominant compensating acceptor in  $n$ -type ZnO, even when grown in Zn-rich conditions. Theoretical approaches consistently indicate that  $V_{\text{Zn}}$  acceptors have a low formation enthalpy when the Fermi level ( $E_F$ ) rises close to the conduction band minimum (CBM) in ZnO [22–24]. Moreover, strong evidence of  $V_{\text{Zn}}$  being the dominant acceptor in ZnO have been reported, including positron

annihilation spectroscopy [25] and luminescence measurements [26].

More precisely, the defect formation enthalpy  $\Delta H_f$  for  $V_{\text{Zn}}$  is given by

$$\Delta H_f(V_{\text{Zn}}^q, \mu, E_F) = E(V_{\text{Zn}}^q) - E_p + \mu + q(E_F + E_{\text{VBM}}) \quad (1)$$

where  $E(V_{\text{Zn}}^q)$  is the total energy of the semiconductor with  $V_{\text{Zn}}$  in a charge state of  $q$ , and  $E_p$  is the energy of the perfect host. Here,  $\mu$ ,  $E_F$ , and  $E_{\text{VBM}}$  are the atomic chemical potential, the Fermi level, and the valence band maximum, respectively. Compared to ZnO,  $\text{Mg}_x\text{Zn}_{1-x}\text{O}$  possesses the same wurtzite structure but a larger bandgap. Since the increased bandgap along with increased Mg content is  $\sim 90\%$  owing to the significantly upward CBM [27], the corresponding  $E_F$  therefore would move up in  $\text{Mg}_x\text{Zn}_{1-x}\text{O}$  alloys accordingly. Based on equation (1), the formation enthalpy of  $V_{\text{Zn}}$  is even lower when  $q < 0$  (i.e.  $V_{\text{Zn}}$  acts as a compensating acceptor) and  $E_F$  rises close to CBM, which is consistent with the previous report [28]. Therefore, it can be expected that  $V_{\text{Zn}}$  will form more easily as Mg composition increases, compensating the free electrons and acting as ionized scattering centers.

Figure 2(b) shows the evolution of  $\mu$  as a function of temperature.  $\mu$  varies slightly over the temperature range, indicating that the dominant scattering mechanism should be temperature independent. Applying the Matthiessen's rule to the degenerated case,  $\mu$  limited by specific scattering mechanisms can be described by

$$\mu^{-1}(n, T) = \mu_I^{-1}(n) + \mu_{\text{PO}}^{-1}(T) + \mu_{\text{AL}}^{-1}(T) + \mu_{\text{BO}}^{-1}(n, T) + \mu_{\text{PE}}^{-1}(n, T) + \mu_{\text{AD}}^{-1}(n, T) \quad (2)$$

where  $\mu_I$ ,  $\mu_{\text{PO}}$ ,  $\mu_{\text{AL}}$ ,  $\mu_{\text{BO}}$ ,  $\mu_{\text{PE}}$ , and  $\mu_{\text{AD}}$  denote ionized impurity scattering, polar optical phonon scattering, alloy scattering, thermionic emission at grain boundaries in degenerate semiconductors, piezoelectric potential scattering, and acoustic deformation potential scattering, respectively. Here,  $n$  and  $T$  represent the carrier concentration and absolute temperature, respectively. The expressions for  $\mu_I$ ,  $\mu_{\text{PO}}$ ,  $\mu_{\text{AL}}$ ,  $\mu_{\text{BO}}$ ,  $\mu_{\text{PE}}$ , and  $\mu_{\text{AD}}$  are given by [16, 26, 29–31]

$$\mu_{\text{PO}}(T) = r_{\text{pop}} \frac{e}{2\alpha\omega_0 m^*} \left[ \exp\left(\frac{\hbar\omega_0}{k_B T}\right) - 1 \right] \quad (3)$$

$$\mu_{\text{AL}}(T) = \frac{(2\pi)^{1/2} e \hbar^4 N}{3(m^*)^{5/2} \sqrt{k_B T} x(1-x)(\Delta E)^2} \quad (4)$$

$$\mu_{\text{BO}}(T) = BT \exp\left(-\frac{\phi_a}{k_B T}\right) \quad (5)$$

$$\mu_{\text{PE}}(n, T) = \frac{2^{3/2} \pi \hbar^2 \varepsilon}{(m^*)^{3/2} P_{\text{pie}}^2 e k_B T} E_f(n)^{1/2} \quad (6)$$

$$\mu_{\text{AD}}(n, T) = \frac{\pi \hbar^4 c_1}{2^{1/2} (m^*)^{5/2} E_1^2 e k_B T} E_f(n)^{-1/2} \quad (7)$$

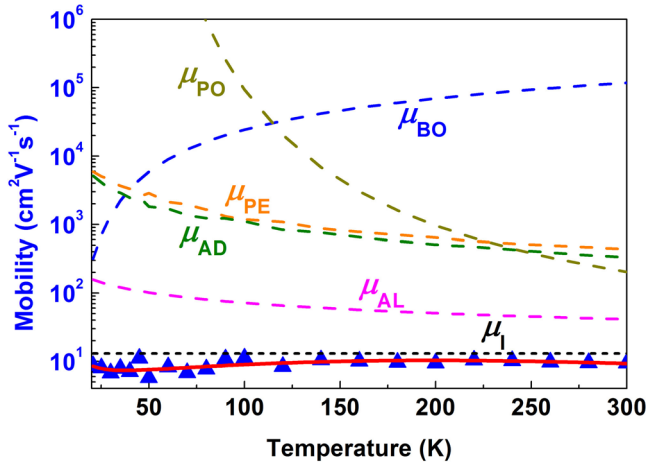


**Figure 3.** (a) Analysis of the temperature-dependent mobility to determine the scattering mechanisms in  $\text{Mg}_{0.12}\text{Zn}_{0.88}\text{O:F}$ . The triangle symbol indicates the measured data. The broken lines show individual electron mobilities limited by ionized impurity scattering ( $\mu_I$ ), polar optical phonon scattering ( $\mu_{\text{PO}}$ ), alloy scattering ( $\mu_{\text{AL}}$ ), thermionic emission at grain boundaries in degenerate semiconductors ( $\mu_{\text{BO}}$ ), piezoelectric potential scattering ( $\mu_{\text{PE}}$ ) and acoustic deformation potential scattering ( $\mu_{\text{AD}}$ ). The red solid line demonstrates the fitting result including all scattering mechanisms based on Matthiessen's rule.

where  $e$ ,  $m^*$ ,  $\hbar\omega_0$ ,  $k_B$ ,  $N$ ,  $x$ ,  $\Delta E$ ,  $\varepsilon$ ,  $P_{\text{pie}}$ ,  $E_f(n)$ ,  $c_1$ , and  $E_1$  denote the elementary charge, the effective mass, the energy of the longitudinal optical phonon, the Boltzmann constant, the number of atoms per unit volume, the fraction of the alloy component, the energy difference between the conduction band edges of ZnO and MgO, the static dielectric constant, the unitless piezoelectric constant (0.21, assume the same as ZnO [30]), the Fermi energy, given by the well-known formula  $E_f(n) = (\hbar^2/2m^*)(3\pi^2n)^{2/3}$  [29], the longitudinal elastic constant ( $1.4 \times 10^{11} \text{ N m}^{-2}$ , assume the same as ZnO [32]) and the deformation potential (3.8 eV, assume the same as ZnO [26]).  $r_{\text{pop}}\phi$  is a slowly varying function of the temperature, which is usually assumed to be 1. The parameter  $B$  is a constant related to the grain size and electron concentration, and  $\phi_a$  represents the activation energy. A set of combinations of  $B$  and  $\phi_a$  was found that fit the experimental results well. The values of the above parameters can be found elsewhere [16, 26, 29–37]. Since  $n$  is temperature independent as illustrated in figure 2(a),  $\mu_I(n)$  could be reasonably assumed a constant in the whole temperature range. Other mechanisms such as dislocation scattering and neutral impurity scattering, which are rarely used in transparent conductors, can be neglected for the heavily doped case [38, 39]. According to the fitting results shown in figure 3,  $\mu$  limited by the ionized impurity scattering is the lowest among the mobilities limited by the specific scatterings. Therefore, the ionized impurity scattering is the dominant mechanism for the low electron mobility in  $\text{Mg}_{0.12}\text{Zn}_{0.88}\text{O:F}$ . Note that Taniyasu *et al* reported a large donor ionization energy of 254 meV and the neutral impurity scattering mechanism in Si-doped AlN [21]. Considering the shallow donor level of F dopants in  $\text{Mg}_x\text{Zn}_{1-x}\text{O}$ , the dominant ionized scattering is physically reasonable in our case. Similar results have been widely found in heavily doped ZnO [40–43].

To quantitatively determine the concentration of ionized scattering centers in  $\text{Mg}_{0.12}\text{Zn}_{0.88}\text{O:F}$ , the formalism of Look *et al* [26] for modeling self-compensation in degenerate semiconductors was adopted. It can be reasonably assumed that F donors are the only dopants and exist as fully ionized  $F_{\text{O}}^+$  donors. Therefore,  $\mu_I$  can be described by Brook–Herring (B–H) theory as

$$\mu_I^{-1}(n) = \mu_{10}^{-1}(n) \frac{\sum Z^2 n_i}{n} = \mu_{10}^{-1}(n) \frac{N_i}{n} \quad (8)$$

where  $n$  and  $N_i$  represent the carrier concentration and the total concentration of ionized impurities of charge  $Z$ , respectively.  $\mu_{10}$  is given by

$$\mu_{10}(n) = \frac{24\pi^3 \varepsilon^2 \hbar^3}{e^3 m^{*2}} \frac{1}{\ln[1 + \Gamma(n)] - \frac{\Gamma(n)}{1 + \Gamma(n)}} \quad (9)$$

where

$$\Gamma(n) = \frac{3^{1/3} 4\pi^{8/3} \hbar^2 n^{1/3} \varepsilon}{e^2 m^*} \quad (10)$$

Here  $\varepsilon$ ,  $\hbar$ ,  $e$ , and  $m^*$  denote the static dielectric constant, the reduced Planck constant, the elementary charge, and the effective mass, respectively. Therefore,  $N_i$  is determined to be  $1.4 \times 10^{20} \text{ cm}^{-3}$ , which is obviously larger than the carrier concentration ( $n = 1.72 \times 10^{19} \text{ cm}^{-3}$ ) and F concentration ( $[F] = 9.0 \times 10^{19} \text{ cm}^{-3}$ ). Thus, the mobility analysis independently confirms the existence of ionized scattering centers other than  $F_{\text{O}}^+$ . Combined with the above analysis of low doping efficiency, it could be concluded that the negatively-charged compensating  $V_{\text{Zn}}^{2-}$  defects partially constitute the ionized scattering centers and thus affect the electron transport.

If  $F_{\text{O}}^+$  and  $V_{\text{Zn}}^{2-}$  are simply considered to be isolated in  $\text{Mg}_{0.12}\text{Zn}_{0.88}\text{O:F}$ , the concentration of  $V_{\text{Zn}}^{2-}$  can be determined via the following two methods independently. Firstly, considering the charge neutrality condition  $n = N_{\text{F}} - 2N_{\text{Zn}}$ , where  $N_{\text{F}}$  and  $N_{\text{Zn}}$  denote the concentration of  $F_{\text{O}}^+$  and  $V_{\text{Zn}}^{2-}$ , respectively,  $N_{\text{Zn}}$  can be calculated as  $3.64 \times 10^{19} \text{ cm}^{-3}$ . Secondly, through the total ionized concentration relation  $N_i = N_{\text{F}} + 4N_{\text{Zn}}$ , we can obtain  $N_{\text{Zn}} = 1.25 \times 10^{19} \text{ cm}^{-3}$ , which is not consistent with the previous result. Note that F atoms start to diffuse around 673 K in ZnO [44], which is well below the growth temperature of 723 K. Therefore, it could be reasonably assumed that F dopants effectively migrate close to  $V_{\text{Zn}}^{2-}$  and forms complexes of  $F_{\text{O}}^+ - V_{\text{Zn}}^{2-}$  during growth. To quantitatively determine the concentrations, the charge neutrality condition and the total ionized concentration relation can be rewritten as

$$n = N_{\text{F}} - 2N_{\text{Zn}} - N_{\text{F-Zn}} \quad (11)$$

$$N_i = N_{\text{F}} + 4N_{\text{Zn}} + N_{\text{F-Zn}} \quad (12)$$

where  $N_{\text{F-Zn}}$  represents the concentration of  $F_{\text{O}}^+ - V_{\text{Zn}}^{2-}$  complexes. Moreover, the conservation of F dopants yields

$$[F] = N_{\text{F}} + N_{\text{F-Zn}} \quad (13)$$

Thus,  $N_{\text{F}}$ ,  $N_{\text{Zn}}$ , and  $N_{\text{F-Zn}}$  are determined to be  $6.66 \times 10^{19} \text{ cm}^{-3}$ ,  $1.26 \times 10^{19} \text{ cm}^{-3}$ , and  $2.34 \times 10^{19} \text{ cm}^{-3}$ , respectively,

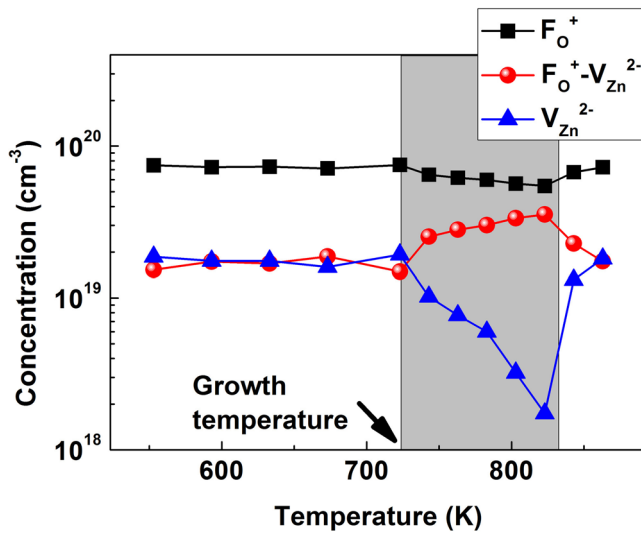


**Figure 4.** Concentrations of  $F_O^+$ ,  $V_{Zn}^{2-}$ , and  $F_O^+-V_{Zn}^{2-}$  complexes as a function of temperature for  $Mg_{0.12}Zn_{0.88}O:F$ .

which are physically reasonable values and comparable with previously reported ones for degenerate ZnO [26, 45]. The total concentration of  $V_{Zn}^{2-}$ -related acceptors ( $N_{Zn} + N_{F-Zn}$ ) exceeds  $3 \times 10^{19} \text{ cm}^{-3}$ , resulting in low doping efficiency.

To investigate the behavior of defects as a function of temperature, the electrical properties of  $Mg_{0.12}Zn_{0.88}O:F$  were characterized in a higher temperature range of 553–863 K.  $n$  and  $\mu$  as a function of temperature were obtained (figure S3 in supplementary materials<sup>6</sup>). Based on equations (11)–(13), the concentrations of defects— $F_O^+$ ,  $V_{Zn}^{2-}$ , and  $F_O^+-V_{Zn}^{2-}$ —were also obtained as a function of temperature, as illustrated in figure 4. The results reveal three regions: (i) below the growth temperature ( $<723 \text{ K}$ ), each of the defects changes slightly, which may be attributed to the low diffusivity of F dopants at low temperatures; (ii) in the range of 723–823 K, F dopants diffuse and form complexes of  $F_O^+-V_{Zn}^{2-}$ , resulting in the decreased concentration of isolated  $F_O^+$  and  $V_{Zn}^{2-}$ . Moreover, the total ionized concentration  $N_i$  decreases from  $1.6 \times 10^{20} \text{ cm}^{-3}$  at 723 K to  $9.7 \times 10^{19} \text{ cm}^{-3}$  at 823 K, indicating reduced ionized scattering to the electron transport. Thus, mobility should increase after complex formation, which is consistent with the measured results (figure S3 in the supplemental material<sup>7</sup>); (iii) F dopants could escape from the sample around 873 K, which well agrees with a previous report [44]. Therefore, the abnormal results above 823 K are attributed to the case that cannot be applicable to equation (13).

The effect of Mg composition on the defects have been further investigated for  $Mg_xZn_{1-x}O:F$  ( $0 \leq x \leq 0.29$ ). As shown in figure 5(a), the concentrations of  $V_{Zn}^{2-}$  and  $F_O^+-V_{Zn}^{2-}$  increase as a function of Mg content, while the concentration of  $F_O^+$  shows the opposite trend. The acceptor/donor concentration ratio  $K = N_A/N_D$  largely increases from 0.23 at  $x = 0$  to 0.47 at  $x = 0.29$ , as illustrated in figure 5(b). Considering that each  $V_{Zn}^{2-}$  can compensate two electrons donated from  $F_O^+$ , the

compensation ratio  $K = 0.47$  at  $x = 0.29$  indicates that over 90% of F dopants become ‘inactive’ in the sample. Thus,  $Mg_xZn_{1-x}O$  would exhibit notably high resistance when the Mg content is even higher ( $x > 0.4$ ), which is consistent with many observations [46–48].

Optical evidence found in CL measurements also verify higher  $V_{Zn}$  concentrations with increased Mg content. As illustrated in figure 6, the peak positions in the near-band-edge (NBE) region exhibit a blueshift as the Mg content increases from  $x = 0$  up to  $x = 0.29$ . More importantly, the peaks related to deep defect emissions are at  $\sim 1.63 \text{ eV}$  and  $\sim 1.89 \text{ eV}$  for ZnO and  $Mg_{0.29}Zn_{0.71}O:F$ , respectively. Dong *et al* pointed out that emission bands in the 1.6–2.1 eV region correlate well with  $V_{Zn}$  concentrations in depth-resolved CL measurements [49], which is in good agreement with our results. The normalization of defect emission peak intensities  $I_D$  to NBE emission intensities  $I_{NBE}$  ( $I_D/I_{NBE}$ ) largely increase from 0.22 for ZnO to 0.90 for  $Mg_{0.29}Zn_{0.71}O:F$ , indicating the increased concentration of  $V_{Zn}$  with increased Mg content [26]. More quantitatively, we might associate the ratio of  $I_D/I_{NBE}$  with the compensation ratio  $K$ .  $I_D/I_{NBE}$  is determined to be 0.22, 0.24, and 0.46 for ZnO,  $Mg_{0.02}Zn_{0.98}O:F$ , and  $Mg_{0.12}Zn_{0.88}O:F$ , respectively, consistent with the corresponding compensation ratio  $K$  (0.23, 0.22, and 0.40, respectively). Exceptionally, the  $I_D/I_{NBE}$  ratio (0.90) is larger than that of  $K$  (0.47) for  $Mg_{0.29}Zn_{0.71}O:F$ , which might be attributed to some factors affecting the recombination process for  $Mg_xZn_{1-x}O$  alloys [50]. Note that other deeper emissions located at  $\sim 2.05 \text{ eV}$  and  $\sim 2.33 \text{ eV}$  are also found for  $Mg_{0.12}Zn_{0.88}O:F$  and  $Mg_{0.29}Zn_{0.71}O:F$ , respectively. For  $Mg_{0.02}Zn_{0.98}O:F$  on the other hand, this emission seems absent, but plausibly exists owing to the non-symmetric peak shape and the unsatisfying fitting result. Considering higher concentrations of  $V_{Zn}^{2-}$  and  $F_O^+-V_{Zn}^{2-}$  complexes with increased Mg content as shown in figure 5(a), this energy level can be assigned to  $V_{Zn}$  clusters or related complexes since the emission energies for vacancy clusters are significantly higher [49].

#### 4. Conclusion

In conclusion, the study of self-compensating defects in  $Mg_xZn_{1-x}O:F$  ( $0 \leq x \leq 0.29$ ) thin films is performed. Based on the theoretical formalism and experimental verification, it is demonstrated that the main cause of the deteriorated conductivity along with increased Mg content is the increased formation of  $V_{Zn}^{2-}$ -related compensating defects in  $Mg_xZn_{1-x}O$  alloys. The compensation ratio  $K$  increases from 0.23 at  $x = 0$  to 0.47 at  $x = 0.29$ , which is further confirmed by CL measurements. The electron transport is mainly limited by ionized impurity scattering. Formation of  $F_O^+-V_{Zn}^{2-}$  complexes could decrease the concentration of ionized scattering centers and thus increase  $\mu$  from  $10 \text{ cm}^2 \text{ V}^{-1} \text{ s}^{-1}$  to  $14 \text{ cm}^2 \text{ V}^{-1} \text{ s}^{-1}$  for  $Mg_{0.12}Zn_{0.88}O:F$ . These results clarify the reason of increasingly high resistivity in  $Mg_xZn_{1-x}O$ , which is a long-sought-after physics problem in this area, and provide crucial information on controlling the conductivity of  $Mg_xZn_{1-x}O$ .

<sup>6</sup> See footnote 3.

<sup>7</sup> See footnote 3.

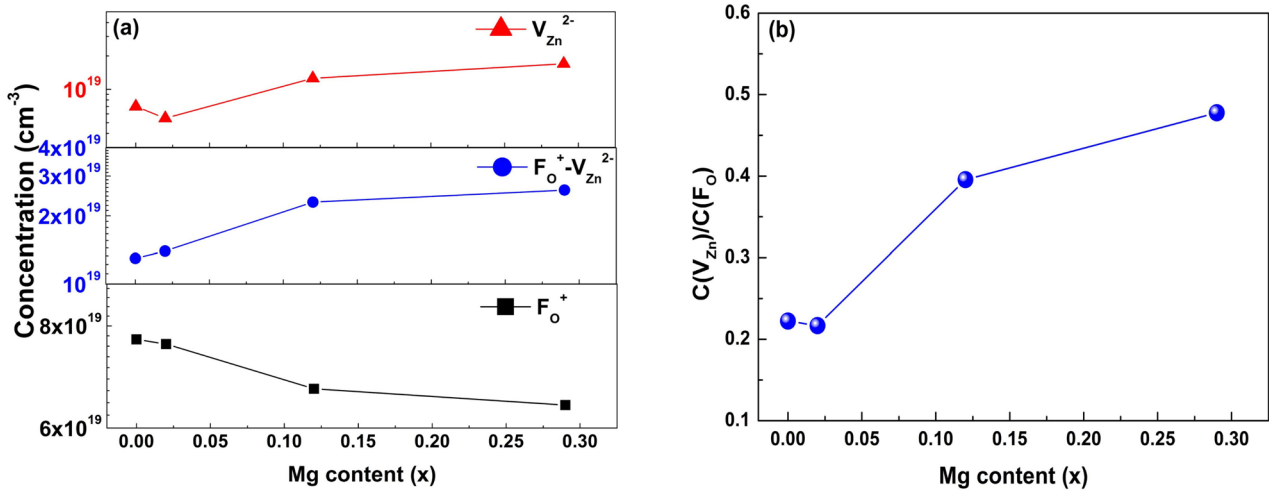


Figure 5. (a) Concentrations of  $F_{\text{O}}^+$ ,  $V_{\text{Zn}}^{2-}$ , and  $F_{\text{O}}^+-V_{\text{Zn}}^{2-}$  complexes and (b) the compensation ratio  $K = N_{\text{A}}/N_{\text{D}}$  as a function of Mg content for  $\text{Mg}_x\text{Zn}_{1-x}\text{O:F}$  ( $0 \leq x \leq 0.29$ ).

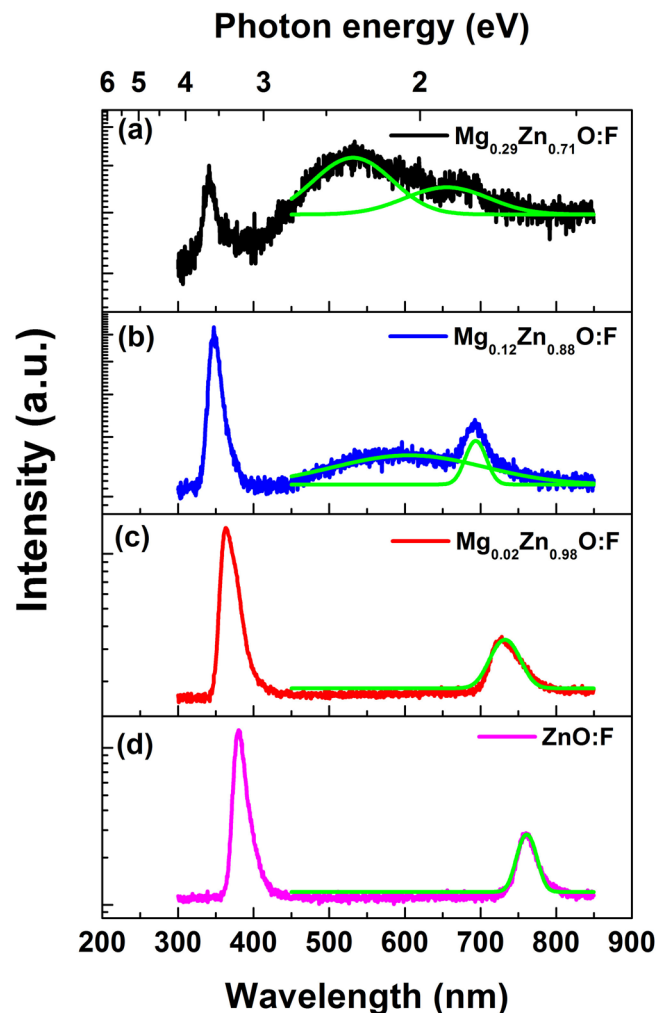


Figure 6. Cathodoluminescence spectra of  $\text{Mg}_x\text{Zn}_{1-x}\text{O:F}$  ( $0 \leq x \leq 0.29$ ) samples at room temperature. The fitting results are also shown.

Moreover, the dopant-defect pairing methodology could be applicable to other wide bandgap semiconductors as well to

improve the performance of high-frequency devices, and thus is of general interest to the semiconductor physics community.

## Acknowledgments

This work was supported by the Ministry of Science and Technology of China (Grants No. 2011CB302002, and No. 2011CB302006), and the National Science Foundation of China (Grants No. 11674405, No. 11274366, No. 61306011, No. 51272280, and No. 11675280).

## References

- [1] Ginley D S and Bright C 2000 *MRS Bull.* **25** 15–8
- [2] Ellmer K 2012 *Nat. Photon.* **6** 809–17
- [3] Özgür Ü, Alivov Y I, Liu C, Teke A, Reshchikov M A, Doğan S, Avrutin V, Cho S-J and Morkoç H 2005 *J. Appl. Phys.* **98** 41301
- [4] Auret F D, Goodman S A, Hayes M, Legodi M J, van Laarhoven H A and Look D C 2001 *Appl. Phys. Lett.* **79** 3074
- [5] Olson D C, Shaheen S E, White M S, Mitchell W J, van Hest M F A M, Collins R T and Ginley D S 2007 *Adv. Funct. Mater.* **17** 264–9
- [6] Hou Y N, Mei Z X, Liu Z L, Zhang T C and Du X L 2011 *Appl. Phys. Lett.* **98** 103506
- [7] Gershon T, Musselman K P, Marin A, Friend R H and MacManus-Driscoll J L 2012 *Sol. Energy Mater. Sol. Cells* **96** 148–54
- [8] Brandt M, von Wenckstern H, Stölzel M, Hochmuth H, Lorenz M and Grundmann M 2011 *Semicond. Sci. Technol.* **26** 14040
- [9] Wei W, Jin C, Narayan J and Narayan R J 2009 *Solid State Commun.* **149** 1670–3
- [10] Lu J G, Fujita S, Kawaharamura T, Nishinaka H, Kamada Y and Ohshima T 2006 *Appl. Phys. Lett.* **89** 262107
- [11] Cohen D J, Ruthe K C and Barnett S A 2004 *J. Appl. Phys.* **96** 459
- [12] Liu L S, Mei Z X, Hou Y N, Liang H L, Azarov A, Venkatachalapathy V, Kuznetsov A and Du X L 2015 *Sci. Rep.* **5** 15516

- [13] Matsubara K, Tampo H, Shibata H, Yamada A, Fons P, Iwata K and Niki S 2004 *Appl. Phys. Lett.* **85** 1374
- [14] Fleischer K, Arca E, Smith C and Shvets I V 2012 *Appl. Phys. Lett.* **101** 121918
- [15] Ma Q-B, He H-P, Ye Z-Z, Zhu L-P, Huang J-Y, Zhang Y-Z and Zhao B-H 2008 *J. Solid State Chem.* **181** 525–9
- [16] Bikowski A and Ellmer K 2013 *J. Appl. Phys.* **114** 63709
- [17] Wei W, Jin C, Narayan J and Narayan R J 2010 *J. Appl. Phys.* **107** 13510
- [18] Liu Z L, Mei Z X, Zhang T C, Liu Y P, Guo Y, Du X L, Hallen A, Zhu J J and Kuznetsov A Y 2009 *J. Cryst. Growth* **311** 4356–9
- [19] Wang X, Saito K, Tanaka T, Nishio M, Nagaoka T, Arita M and Guo Q 2015 *Appl. Phys. Lett.* **107** 22111
- [20] Chand N, Henderson T, Klem J, Masselink W T, Fischer R, Chang Y-C and Morkoç H 1984 *Phys. Rev. B* **30** 4481–92
- [21] Taniyasu Y, Kasu M and Makimoto T 2004 *Appl. Phys. Lett.* **85** 4672
- [22] Janotti A and van de Walle C G 2007 *Phys. Rev. B* **76** 165202
- [23] Vidy R, Ravindran P, Fjellvåg H, Svensson B G, Monakhov E, Ganchenkova M and Nieminen R M 2011 *Phys. Rev. B* **83** 45206
- [24] Lany S and Zunger A 2007 *Phys. Rev. Lett.* **98** 45501
- [25] Tuomisto F, Ranki V, Saarinen K and Look D C 2003 *Phys. Rev. Lett.* **91** 205502
- [26] Look D C, Leedy K D, Vines L, Svensson B G, Zubiaga A, Tuomisto F, Douthett D R and Brillson L J 2011 *Phys. Rev. B* **84** 115202
- [27] Ohtomo A, Kawasaki M, Ohkubo I, Koinuma H, Yasuda T and Segawa Y 1999 *Appl. Phys. Lett.* **75** 980
- [28] Peng H, Scanlon D O, Stevanovic V, Vidal J, Watson G W and Lany S 2013 *Phys. Rev. B* **88** 115201
- [29] Look D C 1989 *Electrical Characterization of GaAs Materials and Devices* (New York: Wiley)
- [30] Rode D L 1975 *Semicond. Semimet.* **10** 1
- [31] Bruneaux J, Cachet H, Froment M and Messad A 1991 *Thin Solid Films* **197** 129–42
- [32] Gopal P and Spaldin N A 2006 *J. Electron. Mater.* **35** 538–42
- [33] Xu Y-N and Ching W Y 1991 *Phys. Rev. B* **43** 4461–72
- [34] Robertson J, Xiong K and Clark S J 2006 *Thin Solid Films* **496** 1–7
- [35] Young D L, Coutts T J, Kaydanov V I, Gilmore A S and Mulligan W P 2000 *J. Vac. Sci. Technol. Vac. Surf. Films* **18** 2978
- [36] Janotti A, Segev D and van de Walle C G 2006 *Phys. Rev. B* **74** 045202
- [37] Janotti A and van de Walle C G 2007 *Phys. Rev. B* **75** 121201
- [38] Ginley D S 2010 *Handbook of Transparent Conductor* (Berlin: Springer)
- [39] Ellmer K and Mientus R 2008 *Thin Solid Films* **516** 4620–7
- [40] Ellmer K 2001 *J. Phys. Appl. Phys.* **34** 3097–108
- [41] Singh A V, Mehra R M, Yoshida A and Wakahara A 2004 *J. Appl. Phys.* **95** 3640
- [42] Brehme S, Fenske F, Fuhs W, Nebauer E, Poschenrieder M, Selle B and Sieber I 1999 *Thin Solid Films* **342** 167–73
- [43] Minami T 2000 *MRS Bull.* **25** 38–44
- [44] Azarov A Y, Svensson B G and Kuznetsov A Y 2012 *Appl. Phys. Lett.* **101** 222109
- [45] Look D C, Leedy K D, Tomich D H and Bayraktaroglu B 2010 *Appl. Phys. Lett.* **96** 62102
- [46] Liu C Y, Xu H Y, Wang L, Li X H and Liu Y C 2009 *J. Appl. Phys.* **106** 73518
- [47] Meher S R, Biju K P and Jain M K 2009 *J. Sol-Gel Sci. Technol.* **52** 228–34
- [48] Hou Y N, Mei Z X, Liang H L, Ye D Q, Gu C Z and Du X L 2013 *Appl. Phys. Lett.* **102** 153510
- [49] Dong Y, Tuomisto F, Svensson B G, Kuznetsov A Y and Brillson L J 2010 *Phys. Rev. B* **81** 081201
- [50] Etacheri V, Roshan R and Kumar V 2012 *ACS Appl. Mater. Interfaces* **4** 2717–25